

Does Face Image Statistics Predict a Preferred Spatial Frequency for Human Face Processing?

Matthias S. Keil*

*Basic Psychology Department, Faculty for Psychology, University of Barcelona (UB),
Passeig de la Vall d'Hebron 171, E-08035 Barcelona (Spain)*

Psychophysical experiments suggested a relative importance of a narrow band of spatial frequencies for recognition of face identity in humans. There exists, however, no conclusive evidence of why it is that such frequencies are preferred. To address this question, I examined the amplitude spectra of a large number of face images, and observed that face spectra generally fall off steeper with spatial frequency compared to ordinary natural images. When external face features (like hair) are suppressed, then whitening of the corresponding mean amplitude spectra revealed higher response amplitudes at those spatial frequencies which are deemed important for processing face identity. The results presented here therefore provide support for that face processing characteristics match corresponding stimulus properties.

Keywords: visual cortex; face recognition; image statistics; whitening; amplitude spectra

Keywords: face recognition, signal statistics, visual system, psychophysics, image processing

I. INTRODUCTION

It has been suggested that the processing of sensory information in the brain has adapted to the specific signal statistics of stimuli ([6]). Such stimulus-specific adaptation is tantamount to taking advantage of statistical regularities in order to encode the highest possible amount of information about the signal ([2, 3, 22, 23, 34]) under various constraints. The constraints include, for example, minimizing energy expenditure ([18, 20, 21]), minimizing wiring costs between processing units ([19]), or reducing spatial and temporal redundancies in the input signal ([1, 2, 5, 17, 28]).

In the case of visual stimuli, natural images reveal a statistical regularity that corresponds to an approximately linear decrease of their amplitude spectra as a function of spatial frequency when scaling both coordinate axis logarithmically ([7, 11]). This property is equivalent to strong pairwise correlations between pairs of luminance values ([35]). It has been proposed that visual neurons utilize this statistical property in a way that cells tuned to different spatial frequencies have equal sensitivities ([11]). Thus, neurons tuned to high spatial frequencies should increase their response gain such that they achieve the same response levels as low frequency neurons. This is the *response equalization hypothesis* (which should be distinguished from the *decorrelation hypothesis*) ([1, 14, 28]). Response equalization (“whitening”) may enhance the information throughput from one neuronal stage to another by adjusting the output of one stage such that it matches the limited dynamic range of the successive stage ([14]).

The present article unveils a link between statistical properties of face images and psychophysical data for the processing of face identity. The processing of face identity

was found to preferably depend on a narrow spatial frequency band (about 2 octaves) from 8 to 16 cycles per face ([9, 10, 12, 16, 24, 25, 26, 30]). However, to the best of my knowledge, no explanation has been offered yet of why it is that face processing mechanisms in the human brain reveal such a preference.

Here I analyzed the amplitude spectra of a large number of face images. Different types of amplitude spectra were considered - with and without suppression of external face features (hair, shoulders, etc.). The spectra were whitened (i.e., “response”-equalized) according to three different procedures. In this way it is demonstrated that the main results are largely independent of the specific method that was used for whitening: amplitudes were higher at spatial frequencies around 10 cycles per face - but only in those spectra where external face features were suppressed. Therefore, the effect must have been produced by internal face features (eyes, mouth, nose).

II. RESULTS

Amplitude spectra

Amplitude spectra are best conceived in polar coordinates, where the spatial frequency k varies proportional to radius. Thus, spectral amplitudes which have the same spatial frequency lie on a circle. The 2-D spectrum can be collapsed into an 1-D isotropic spectrum for each k by averaging all amplitudes on that circle. This means that in an isotropic spectrum any orientation dependence of the amplitudes is lost.

The amplitude spectra of *natural* images were found to depend on spatial frequency as $\propto k^\alpha$, with an average (isotropic) spectral slope $\alpha \approx -1$ ([7, 11]).

How do the amplitude spectra of face images compare to this finding? To answer, I computed slopes of the amplitude spectra of 868 female and 868 male face images (size 256×256). In a double-logarithmic representation,

*Electronic address: mats@cvc.uab.es

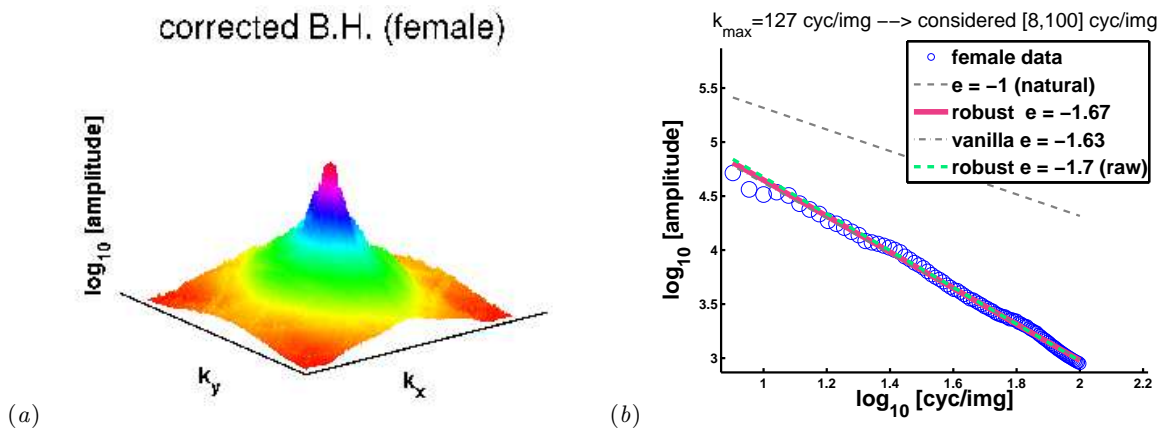


FIG. 1: **Corrected Blackman-Harris spectrum (females).** (a) Logarithmized, mean amplitude spectrum of all female face images. Prior to computing individual spectra, a Blackman-Harris (B.H.-) window was applied to each face image in order to suppress external face features (Supp. Fig. 7d). The application of the B.H.-window, however, leaves an undesired spectral “fingerprint” in each of the spectra (Supp. Fig. 5a), which was attenuated before averaging (Supp. Fig. 6).

(b) The 2-D spectrum shown on the left is transformed into a 1-D isotropic spectrum by averaging all amplitudes with different orientations at a fixed frequency k ($=$ circle symbols). The size of each circle symbol is proportional to the standard deviation (s.d.). The maximum s.d. (biggest circle) was 9186.75 (39.3%), and the minimum s.d. (smallest circle) was 252.67 (28.08%). In the legend, e denotes slope values α (i.e., $\alpha \equiv e$). For comparison, the typical slope of *natural* images ($e = -1$) is also shown as a dashed gray line. The label “*vanilla*” refers to line fitting with an ordinary linear regression (least square fit) algorithm for computing slopes. Since linear regression is sensitive to outliers, slope values were additionally computed with an outlier-insensitive ($=$ *robust*) algorithm. Finally, the slope for the uncorrected (“raw”) amplitude spectrum is also indicated.

gender	averaging of:	raw	corr.raw	B.H.	corr.B.H.
female	<i>slopes</i>	-1.608 ± 0.0858	-1.604 ± 0.0870	-1.686 ± 0.0698	-1.654 ± 0.0731
	<i>spectra</i>	-1.584	-1.579	-1.701	-1.668
male	<i>slopes</i>	-1.649 ± 0.0738	-1.645 ± 0.0757	-1.673 ± 0.0785	-1.642 ± 0.0895
	<i>spectra</i>	-1.644	-1.637	-1.689	-1.658

TABLE I: For each gender, the table shows the average slope values for the four types of amplitude spectra. Two possibilities for computing these values were considered: “*slopes*” means that individual slope values were averaged (each gender $n = 868$, c.f. Supp. Fig. 9), and “*spectra*” refers to the slope of the average spectrum as illustrated with Figure 1(a).

these spectra also decreased approximately linear as a function of spatial frequency (Figure 1). Therefore a line with (spectral) slope α could be fitted to each spectrum. Four different types of amplitude spectra were considered for each face image (with different α , see table I and methods section).

At first the spectra of the original images were computed (“raw”). The second type of spectrum is defined by attenuating in each spectrum the truncation artifacts (“corr. raw”, Supp. Fig. 5c and Supp. Fig. 6). These artifacts are a consequence of the cropped shoulder region being displayed in each image besides the actual face. To smoothly strip off external face features (like the hair, i.e. anything but the actual face), a Blackman-Harris window was applied to each image prior to computing its spectrum (“Blackman-Harris” or “B.H.” – see Supp. Fig. 7d). Because application of the B.H.-window leaves a faint but characteristic spectral “fingerprint” (Supp. Fig. 5a), a further spectrum type (“corr. B.H.”) was considered, with the artificial “fingerprint” being attenuated.

The mean isotropic slope values were computed in two

ways. First, the spectral slope of each face image was computed, and individual slope values were averaged (label “*slopes*” in table I). Second, an average spectrum is computed at first, which is composed of all individual spectra (see Figure 1). The second slope value corresponds then to the slope of the average spectrum (label “*spectra*” in table I). Isotropic slope values are situated around -1.6 , with minima and maxima of -2.014 & -1.180 (females), respectively, and -1.994 & -1.007 (males).

Notice that the standard deviations associated with the slopes of arbitrary natural images are usually bigger ([31, 33]), as there is no restriction on displayed content and scale, respectively ([32]).

Usually, α varies also as a function of orientation Θ ([29, 33]). The orientation dependence is illustrated by means of the averaged corrected spectra (Figure 2). Minimum slope values are located at 0° (wave vector pointing to east) and 90° (north), respectively, whereas maxima tend to be at oblique orientations. Slope values of the B.H. spectra vary more than with the raw spectra. As external features are widely suppressed in the B.H. spec-

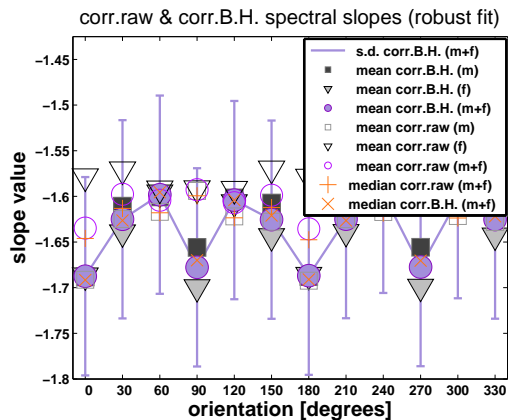


FIG. 2: **Oriented spectral slope.** The curves juxtapose oriented spectral slopes from corrected raw (“corr.raw”) spectra and corrected Blackman-Harris-windowed (“corr.B.H.”) spectra (see legend). Slopes were computed from the respective averaged spectra, with angular increments of 30° ([33]). Error bars denote ± 1 standard deviation (estimated using robust statistics). Uncorrected spectra show similar dependencies of slopes from orientation. Notice that slope values are defined modulus 180° .

tra, minimum slopes are associated with the orientations of the internal face features ($0^\circ, 180^\circ$: nose; $90^\circ, 270^\circ$: eyes, mouth, and the bottom termination of the nose). Summarizing so far, the majority of the individual α for face images is more negative than the theoretically predicted lower bound of -1.5 for natural images ([4]) (table I; Supp. Fig. 9). Similar observations also hold for spectral slopes of the mean amplitude spectra (Figure 1). This should not come as a surprise since the structure of face images is different from natural images: face images are not composed of self-occluding, constant intensity surface patches ([4, 27]), and lack the self-similar distribution of spectral energy as it was reported for natural images ([11]).

Whitening the Amplitude spectra

Here I ask whether by amplitude equalization of amplitude spectra (“whitening”) one could explain psychophysical data on face perception. The results which are presented below were obtained with the mean spectra.

Consider first the isotropic (1-D) spectra. Because the spectra fall, as a function of spatial frequency k , as $\propto k^{-|\alpha|}$, we can multiply amplitudes by $k^{|\alpha|}$ to obtain a “flat” spectrum (in the sense that its Shannon entropy is maximal). The slopes which were used to this end are the “spectra” ones from table I. Whitened 1-D spectra are shown in Figure 3. They are not completely flat, but instead have a global maximum at around 10 cycles per face, and a second but local maximum at around 30 cycles per face.

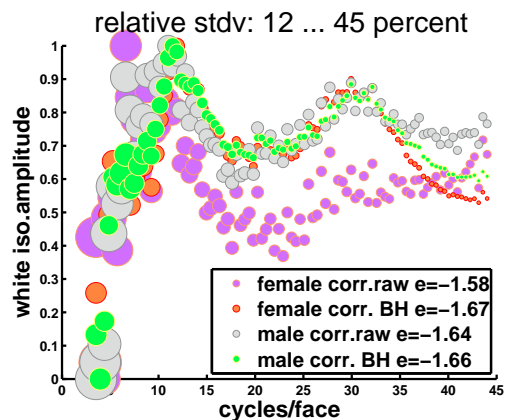


FIG. 3: **1-D whitening.** Whitening of the corrected mean, isotropic 1-D spectra reveals a global amplitude maximum at ≈ 10 cycles per face with all four spectra (see legend). Symbol size is proportional to standard deviation (relative values are indicated in the figure). The slopes which were used for whitening are indicated in the legend (c.f. table I).

Consider now the 2-D spectra, where whitening was carried out according to three different procedures: whitening by *slopes* (analogous to the 1-D case), by *variance*, and by *diffusion* (see methods section). Results are shown in Figure 4 for females, and in Supp. Fig. 10 for males. For both genders, the whitened B.H.-spectra reveal amplitude maxima only within a narrow band of low spatial frequencies. Furthermore, frequency maxima appear only at a specific orientation in the spectra which corresponds to horizontally oriented face features (“horizontal amplitudes”, i.e. eyes and mouth). These results are obtained independently from the specific whitening procedure which was used (*slope*-whitening: Figure 4a & Figure 10a; *variance*-whitening: Supp. Fig. 11; *diffusion*-whitening: not shown).

Plotting of only these “horizontal amplitudes” (indicated by a white box in Figure 4a) for all three whitening procedures allows to identify the spatial frequencies of the maxima with higher precision. The curves now show clearly that the maxima occur in the range from 10 to 15 cycles per face height. Nevertheless, maxima are only revealed by whitening of the B.H.-windowed spectra, but not by whitening of any raw spectra. This means that amplitude enhancement due to internal face features is annihilated by the presence of external face features (such as hair or shoulder).

III. DISCUSSION

Here, I studied amplitude spectra of face images in the context of response equalization (whitening). Were external face features (hair, shoulder) suppressed by windowing the face images with a Blackman-Harris window, then amplitude maxima are observed in the whitened spectra at low spatial frequencies. For the isotropic 1-D spec-

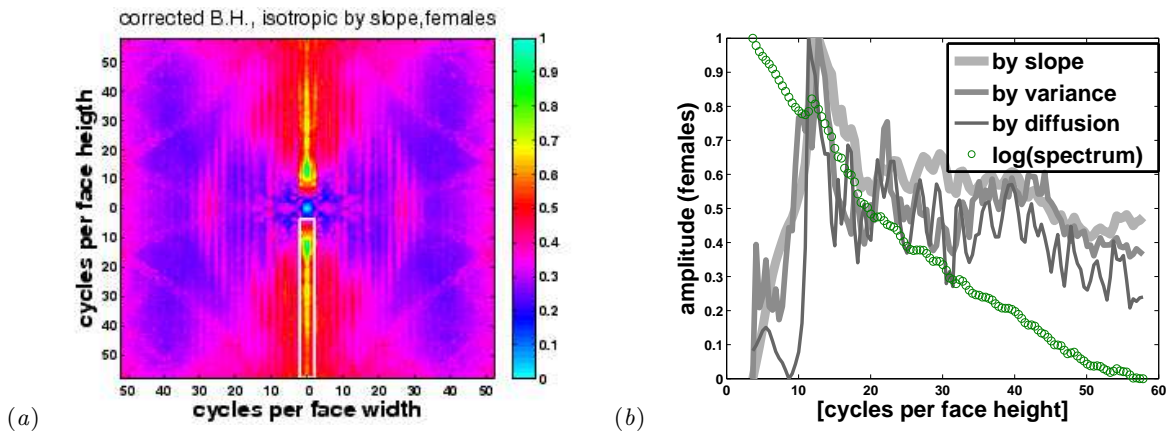


FIG. 4: **2-D whitening.** (a) Slope-whitening of the mean corrected B.H.-spectra unveiled clear maxima at horizontal feature orientations (marked by a white box). Here the female data are shown (male data: Supp. Fig. 10). (b) The curves show the amplitudes at the location demarcated by the white box in the spectrum: “*log(spectrum)*” are the logarithmized amplitudes without whitening; amplitudes whitened “*by slope*”, “*by variance*”, and “*by diffusion*” (see methods sections for further details on the three whitening procedures). The important result here is that whitened amplitudes reveal a distinct maxima irrespective of the specific whitening method at $\approx 10 - 15$ cycles per face height. The variance-whitened spectra are shown in Supp. Fig. 11.

tra, maxima are situated around 10 cycles per face, and for the 2-D spectra at around 10 – 15 cycles per face height. In the 2-D case, three different whitening methods yielded consistent results.

Several psychophysical studies suggest that recognition of face identity works *best* in a narrow band (bandwidth about 2 octaves) of spatial frequencies from ≈ 8 to ≈ 16 cycles per face ([9, 12, 13, 16, 24, 26, 30]). Notice that this does not mean that face recognition exclusively depends on this frequency band, as faces can still be recognized when corresponding frequency information is suppressed ([24, 25]).

Because the amplitude maxima appear in the whitened spectra exclusively at horizontal feature orientations, my results suggest that the psychophysical frequency preference might have been caused by an adaptation of corresponding neuronal mechanisms to eyes and mouth.

Interestingly, in the earlier cited psychophysical studies the spatial frequencies are often measured in “cycles per face width” (i.e., along vertically oriented face features), whereas the results presented here were rather brought about by horizontally oriented face features. The factors to convert spatial frequencies from “cycles per image” to “cycles per face” (see methods) are statistically different for width and height (as suggested by a one-way ANOVA and a Kruskal-Wallis test). However, they are not so different in absolute terms. The aforementioned frequency interval of 10 – 15 *cycles per face height* transforms into $\approx 9 - 13.5$ *cycles per face width* for females and $\approx 9 - 13.6$ *cycles per face width* for males, respectively, what is still in good agreement with the psychophysical data.

Psychophysical thresholds for face recognition are not significantly affected by the structure of the background in which a face is embedded ([8]). Therefore, although the faces used in this study are shown against an uniform background, the validity of results should extend

to arbitrary backgrounds. Notice, however, that amplitude spectra consider the complete frequency content of an image, whereas humans have attentional mechanisms which allows them to process only a region of interest, and ignore background effects. Windowing the face images with a Blackman-Harris window achieves the the same computational purpose: anything but the internal face features are suppressed. A follow-up paper examines in more detail the properties of internal face features by means of a model of simple and complex cells.

The statistical prediction of a preferred band of spatial frequencies may also have implications for artificial face recognition systems. Future experiments should systematically address the question whether the recognition performance of artificial systems is optimal at spatial frequencies similar to those used by humans.

Methods

Face images. We used 868 female face images, and 868 male face images from the *Face Recognition Grand Challenge* database (FRGC, <http://www.frvt.org/FRGC> or www.bee-biometrics.org). Original images (1704×2272 pixels, 24-bit true color) were adjusted for horizontal alignment of eyes, before they were down-sampled to 256×256 pixels and converted into 8-bit grey-scale. Subsequently, the positions of left eye, right eye, and mouth $[(x_{le}, y_{le}), (x_{re}, y_{re}), \text{ and } (x_{mouth}, y_{mouth})]$, respectively] were manually marked by two persons (M.S.K. and E.C.) with an *ad hoc* programmed graphical interface. The position of each face center (\approx nose) was approximated as $x_{nose} = \text{rnd}((x_{le} + x_{re})/4 + x_{mouth}/2)$ and $y_{nose} = \text{rnd}[0.95 * \text{rnd}(y_{le} + (y_{mouth} - (y_{le} + y_{re})/2)/2)]$, where $\text{rnd}(\cdot)$ denotes rounding to the nearest integer value.

Dimension of spatial frequency. For conversion of spatial frequency units, face dimensions were manually marked with an *ad hoc* programmed graphical interface. The factors for multi-

plying “cycles per image” to obtain “cycles per face width” were 0.41 ± 0.013 (females, $n = 868$) and 0.43 ± 0.012 (males, $n = 868$). Corresponding factors for obtaining “cycles per face height” were 0.46 ± 0.021 (females) and 0.47 ± 0.018 (males). Conversion factors at oblique orientations were calculated under the assumption that horizontal and vertical conversion factors define the two main axis of an ellipse. Pooling of results over gender implied also a corresponding averaging of conversion factors, and the factors for width and height were averaged in the isotropic case.

Amplitude spectra. Let the features which are not part of the actual face be denoted by *external features* (e.g., shoulder region or hair). On the other hand, *internal features* refer to the eyes, the mouth, and the nose. The presence of external features in our face images influences in their amplitude spectra, and may cause truncation artifacts. It is thus desirable to compare results with and without the presence of external features. A good suppression of external features could be achieved by centering a *minimum 4-term Blackman-Harris window* ([15]) at (x_{nose}, y_{nose}) (Supp. Fig. 7 & 8). Nevertheless, application of the window leaves a characteristic “fingerprint” in each spectrum (Supp. Fig. 5a). This artificial “fingerprint”, as well as the spurious lines caused by truncation, could be attenuated with a correction procedure based on a spatially varying diffusion mechanism (outlined below). Thus, for each face image, originally four types of amplitude spectra were considered: the original “raw” spectrum, the “Blackman-Harris”-spectrum, and their respective corrected versions (i.e., “corr. raw” and “corr. B.H.”).

Correction of Amplitude Spectra. Let $P \in \{0, 1\}^{n \times n}$ be a binary $n \times n$ matrix of the same size as the 2-D amplitude spectra \mathcal{A} . In P , artifacts are represented by ones, while all other positions are set to zero. Thus, P is set to the image shown in Supp. Fig. 5(b) for correcting the Blackman-Harris spectrum, and Supp. Fig. 5(c) for the raw spectrum. The idea of the correction algorithm consists in simply averaging out the positions with artifacts. To this end, information from neighboring positions flows into artifact positions. This process is called *inward diffusion*. Let $\mathcal{X}(t)$ be a sequence of corrected amplitude spectra parameterized over time t , with the initial condition $\mathcal{X}(0) \equiv \mathcal{A}$. Inward diffusion is defined by $\partial \mathcal{X}_{ij} / \partial t = P_{ij} \nabla^2 \mathcal{X}_{ij}$, where (i, j) denotes matrix positions. The diffusion process was terminated at the moment when the *correlation difference* $c(t) - c(t + \Delta t)$ was smaller than 0.001, or when a maximum of 100 iterations were done.

Slopes of amplitude spectra. *Isotropic slopes α :* Amplitudes associated with a given spatial frequency lie on a circle. This is to say that when representing the spectrum with polar coordinates, then spatial frequencies vary along the radial coordinate, but stay constant while varying orientation. An isotropic amplitude spectra is obtained by averaging all amplitudes with a fixed spatial frequency across orientations (i.e., for each circle, the mean value of all amplitudes of the circle was computed). Because the logarithmized amplitude spectra of face images fall approximately linear as a function of log-frequency, a line with slope α could be fitted to the

isotropic spectra. Although in principle amplitude data were available from $k = 1$ to $k = 127$ cycles per image, only the interval from $k_{min} = 8$ to $k_{max} = 100$ was used for line fitting. I used the function “*robustfit*” (linear regression with low sensitivity to outliers) provided with Matlab’s statistical toolbox (*Matlab* version 7.1.0.183 R14 SP3, *Statistical Toolbox* version 5.1, see www.mathworks.com). *Oriented spectral slopes $\alpha(\Theta)$* (Figure 2): Each 2-D amplitude spectrum was subdivided into 12 “pie slices” (each with $\Delta\Theta = 30^\circ$). For each pie slice with orientation Θ , an (oriented) isotropic 1-D spectrum was analogously computed as just described (with amplitudes being averaged across arcs), and subsequently a line with slope $\alpha(\Theta)$ was fitted.

Slope-Whitening of Amplitude Spectra. This algorithm proceeds in straight analogy to whitening of the isotropic spectra. Let α be the isotropic slope value corresponding to a 2-D amplitude spectrum $\mathcal{A}(k_x, k_y)$ with spatial frequency coordinates $k_x, k_y \in [1, 127]$ cycles per image. Let $k = \sqrt{k_x^2 + k_y^2}$ (radial spatial frequency). Then, the corresponding whitened spectrum \mathcal{W} is defined as $\mathcal{W}(k_x, k_y) = \mathcal{A}(k_x, k_y) \cdot k^{|\alpha|}$. Qualitatively, the \mathcal{W} were not different from a more advanced procedure that consisted in subdividing \mathcal{A} into oriented “pie slices” and whitening each with its corresponding oriented slope value $\alpha(\Theta)$. Therefore, only those results are presented where \mathcal{A} was whitened with an isotropic slope value (the term “isotropic” in the headline of the spectra in Figure 4 and Supp. Fig. 10 indicates just this).

Whitening by Variance. Amplitudes in the spectrum $\mathcal{A}(k_x, k_y)$ with equal spatial frequencies lie on a circle with radius $k = \sqrt{k_x^2 + k_y^2}$. Let n_k be the number of points on this circle (n_k monotonically increases as a function of k). Let $\mathcal{A}(k, \Theta)$ be the spectrum in polar coordinates. Then, we first average, for each k , all amplitudes across orientations according to $\mu(k) = \sum_{\Theta} \mathcal{A}(k, \Theta) / n_k$. The variance is subsequently computed as $\sigma^2(k) = \sum_{\Theta} (\mathcal{A}(k, \Theta) - \mu(k))^2 / (n_k - 1)$. Finally, the variance-whitened spectrum is defined as $\mathcal{V} = \mathcal{A} / (\sigma^2(k) + \epsilon)$ with a small positive constant $\epsilon \ll 1$. Examples of \mathcal{V} are shown in Supp. Fig. 11.

Whitening by Diffusion. Let $\mathcal{X}(k_x, k_y, t)$ a sequence of amplitude spectra parameterized over time t , with the initial condition $\mathcal{X}(k_x, k_y, 0) \equiv \mathcal{A}(k_x, k_y)$. For $t > 0$, the \mathcal{X} are defined according to the diffusion equation $\partial \mathcal{X} / \partial t = \nabla^2 \mathcal{X}$. The whitened spectrum then is $\mathcal{D} \equiv \mathcal{A} / (1 + \mathcal{X}(t_{max}))$ at precisely the instant t_{max} when the Shannon entropy of \mathcal{D} is maximal.

Acknowledgements

This work was partially supported by the *Juan de la Cierva* program from the Spanish Government (BKC-IYK-6707). Further support was granted by the MCyT grant SEJ 2006-15095. M.S.K. wishes to thank Esther Calderón for her valuable help in acquiring feature positions, as well as Hans Supèr for helpful comments.

[1] Atick, J. and Redlich, A. 1992. What does the retina know about natural scenes? *Neural Computation*, 4:196–

- [2] Attneave, F. 1954. Some informational aspects of visual perception. *Psychological Review*, 61(3):183–193.
- [3] Baddeley, R., Abbott, L., Booth, M., Sengpiel, F., and Freeman, T. 1998. Responses of neurons in primary and inferior temporal visual cortices to natural scenes. *Proceedings of the Royal Society, London B*, 264:1775–1783.
- [4] Balboa, R. and Grzywacz, N. 2001. Occlusions contribute to scaling in natural images. *Vision Research*, 41:955–964.
- [5] Barlow, H. 1961. Possible principles underlying the transformation of sensory messages. In Rosenblith, W., editor, *Sensory Communication*, pages 217–234. MIT Press, Cambridge, MA.
- [6] Barlow, H. 1989. Unsupervised learning. *Neural Computation*, 1:295–311.
- [7] Burton, G. and Moorhead, I. 1987. Color and spatial structure in natural scenes. *Applied Optics*, 26(1):157–170.
- [8] Collin, C., Wang, K., and O’Byrne, B. 2006. Effects of image background on spatial-frequency threshold for face recognition. *Perception*, 35:1459–1472.
- [9] Costen, N., Parker, D., and Craw, I. 1994. Spatial content and spatial quantisation effects in face recognition. *Perception*, 23:129–146.
- [10] Costen, N., Parker, D., and Craw, I. 1996. Effects of high-pass and low-pass spatial filtering on face identification. *Perception and Psychophysics*, 58:602–612.
- [11] Field, D. 1987. Relations between the statistics of natural images and the response properties of cortical cells. *Journal of the Optical Society of America A*, 4(12):2379–2394.
- [12] Fiorentini, A., Maffei, L., and Sandini, G. 1983. The role of high spatial frequencies in face perception. *Perception*, 12:195–201.
- [13] Ginsburg, A. 1978. *Visual information processing based on spatial filters constrained by biological data*. PhD thesis, Cambridge University, Cambridge, England.
- [14] Graham, D., Chandler, D., and Field, D. 2006. Can the theory of “whitening” explain the center-surround properties of retinal ganglion cell receptive fields? *Vision Research*, 46(18):2901–2913.
- [15] Harris, F. 1978. On the use of windows for harmonic analysis with the discrete Fourier transform. *Proceedings of the IEEE*, 66(1):51–84.
- [16] Hayes, A., Morrone, M., and Burr, D. 1986. Recognition of positive and negative band-pass filtered images. *Perception*, 15:595–602.
- [17] Hosoya, T., Baccus, S., and Meister, M. 2005. Dynamic predictive coding by the retina. *Nature*, 436:71–77.
- [18] Laughlin, S., de Ruyter van Steveninck, R., and Anderson, J. 1998. The metabolic cost of neural information. *Nature Neuroscience*, 1(1):36–41.
- [19] Laughlin, S. and Sejnowski, T. 2003. Communication in neural networks. *Science*, 301:1870–1874.
- [20] Lenny, P. 2003. The cost of cortical computation. *Current Biology*, 13:493–497.
- [21] Levy, W. and Baxter, R. 1996. Energy-efficient neural codes. *Neural Computation*, 8:531–543.
- [22] Linsker, R. 1988. Self-organization in a perceptual network. *IEEE Transactions on Computer*, 21(3):105–117.
- [23] Nadal, J.-P., Brunel, N., and Parga, N. 1998. Nonlinear feedforward networks with stochastic outputs: Infomax implies redundancy reduction. *Network: Computation in Neural Systems*, 9:1–11.
- [24] Näsänen, R. 1999. Spatial frequency bandwidth used in the recognition of facial images. *Vision Research*, 39:3824–3833.
- [25] Ojanpää, H. and Näsänen, R. 2003. Utilisation of spatial frequency information in face search. *Vision Research*, 43(24):2505–2515.
- [26] Peli, E., Lee, E., Trempe, C., and Buzney, S. 1994. Image enhancement for the visually impaired: the effects of enhancement on face recognition. *Journal of the Optical Society of America A*, 11:1929–1939.
- [27] Ruderman, D. 1997. Origins of scaling in natural images. *Vision Research*, 37(23):3385–3398.
- [28] Srinivasan, M., Laughlin, S., and Dubs, A. 1982. Pre-

dictive coding: a fresh view of inhibition in the retina. *Proceedings of the Royal Society of London B*, 216:427–459.

- [29] Switkes, E., Mayer, M., and Sloan, J. 1978. Spatial frequency analysis of the visual environment: anisotropy and the carpentered environment hypothesis. *Vision Research*, 18:1393–1399.
- [30] Tieger, T. and Ganz, L. 1979. Recognition of faces in the presence of two-dimensional sinusoidal masks. *Perception and Psychophysics*, 26:163–167.
- [31] Tolhurst, D., Tadmor, Y., and Chao, T. 1992. Amplitude spectra of natural images. *Ophthalmic and Physiological Optics*, 12:229–232.
- [32] Torralba, A. and Oliva, A. 2003. Statistics of natural image categories. *Network: Computation in Neural Systems*, 14:391–412.
- [33] van der Schaaf, A. and van Hateren, J. 1996. Modelling the power spectra of natural images: statistics and information. *Vision Research*, 36(17):2759–2770.
- [34] Wainwright, M. 1999. Visual adaptation as optimal information transmission. *Vision Research*, 39:3960–3974.
- [35] Wiener, N. 1964. *Extrapolation, Interpolation, and Smoothing of Stationary Time Series*. The MIT Press, Cambridge, Massachusetts.

Supplementary Figures

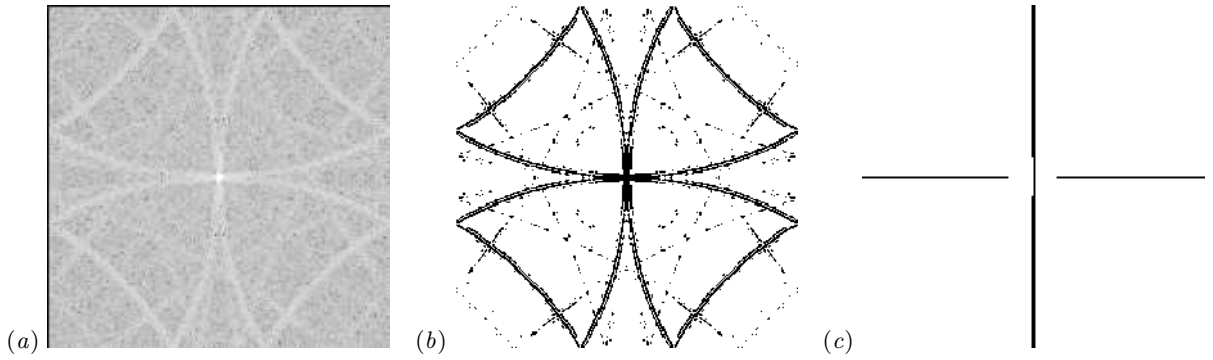


FIG. 5: **Artifacts in the amplitude spectra.** (a) The log-amplitude-spectrum of the *minimum 4-term Blackman-Harris* (B.H.) window reveals a characteristic “fingerprint” (shown in this image), which also emerges when averaging a big number of amplitude spectra of B.H.-windowed faces. (b) The “fingerprint” is transformed into a binary image by thresholding with -0.25 (black color indicates values with 1, and white indicates 0). (c) Manually marked line artifacts which appear by averaging the amplitude spectra of a big number of face images (here without windowing).

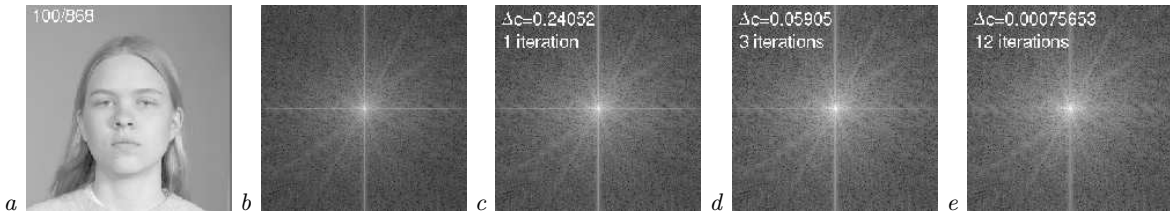


FIG. 6: **Suppressing artifacts in the amplitude spectra.** This figure illustrates how artifacts in the amplitude spectra are suppressed by a nonlinear diffusion process, where the thresholded images of Supp. Fig. 5 served as spatially variant diffusion coefficient (see methods section). (a) Original face image. (b) The log-amplitude-spectrum of the image has horizontal and vertical lines which are generated as a consequence of truncating the shoulder region (c.f. Supp. Fig. 5c). (c) The spectrum after one iteration of nonlinear diffusion, with a difference in correlation to the original spectrum $\Delta c(1) \equiv c(0) - c(1) = 0.24052$. The spurious lines are already attenuated. (d) Three iterations with $\Delta c(3) = 0.05905$. (e) 12 iterations with $\Delta c(12) < 0.001$, which is the stopping criterion. The artificial lines are largely suppressed. The rest of the amplitude spectrum remains intact, and more interesting structures are now visible.

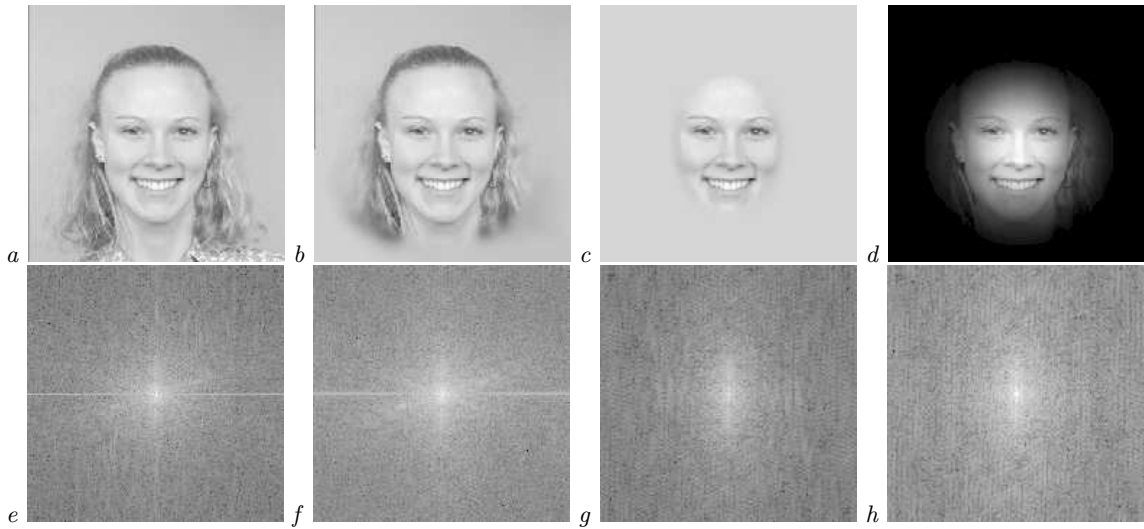


FIG. 7: **Suppression of external face features.** The images in the bottom row ($e-h$) show the logarithmized amplitude spectra of the images ($a-d$) (face ID 104). The amplitude spectrum (e) of the original image (a) shows spurious horizontal and the vertical lines. (b) The spurious vertical line disappeared in the amplitude spectrum (f) when the shoulder region was manually erased, and the horizontal line then had a smaller amplitude. (c) Erasing all external face features led to the creation of a “moonface”, thereby suppressing all of the artificial lines (g). Finally, in (d), a *minimum 4-term Blackman-Harris window* was centered at the nose position of the original image. The corresponding amplitude spectrum (h) of the windowed image is very similar to the amplitude spectrum of the “moonface” spectrum (but see Supp. Fig. 8).

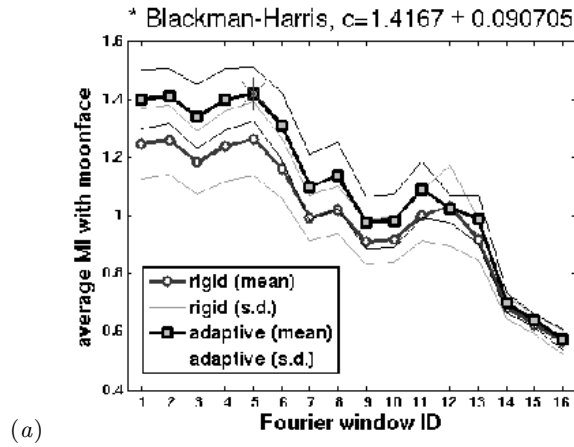


FIG. 8: **Similarities between the logarithmized amplitude spectra of “moonfaces” and windowed faces.** For six selected female images which revealed strong line artifacts in their amplitude spectra, I computed similarity measures between the logarithmized amplitude spectra of corresponding “moonfaces” (e.g., Supp. Fig. 7g) and windowed faces (e.g., Supp. Fig. 7h; the window type is specified by the numbers at the abscissae). The plot shows mutual information averaged across the the six images (mean \pm s.d.). The center of the window was either positioned always at the center position of each image (“rigid”), or at the nose position with variable radius (“adaptive”) – see legend. The *minimum 4-term Blackman-Harris window* scored the highest similarity (indicated by a red star). With correlation instead of mutual information, the curves show nearly the same relative similarities. In that case, the maximum average correlation value (\pm s.d.) was 0.87 ± 0.02 again for the adaptive *minimum 4-term Blackman-Harris window*.

The identification numbers (“Fourier-IDs”) of the windows were 1=*Chebyshev window*, 2=*Nuttall-defined minimum 4-term Blackman-Harris window*, 3=*Bohman window*, 4=*Parzen (de la Valle-Poussin) window*, 5=*minimum 4-term Blackman-Harris window*, 6=*Blackman window*, 7=*modified Bartlett-Hann window*, 8=*Hann (Hanning) window*, 9=*triangular window*, 10=*Bartlett window*, 11=*Gaussian window*, 12=*flat top weighted window*, 13=*Hamming window*, 14=*Tukey (tapered cosine) window*, 15=*Kaiser window*, 16=*sharp-edged disk*.

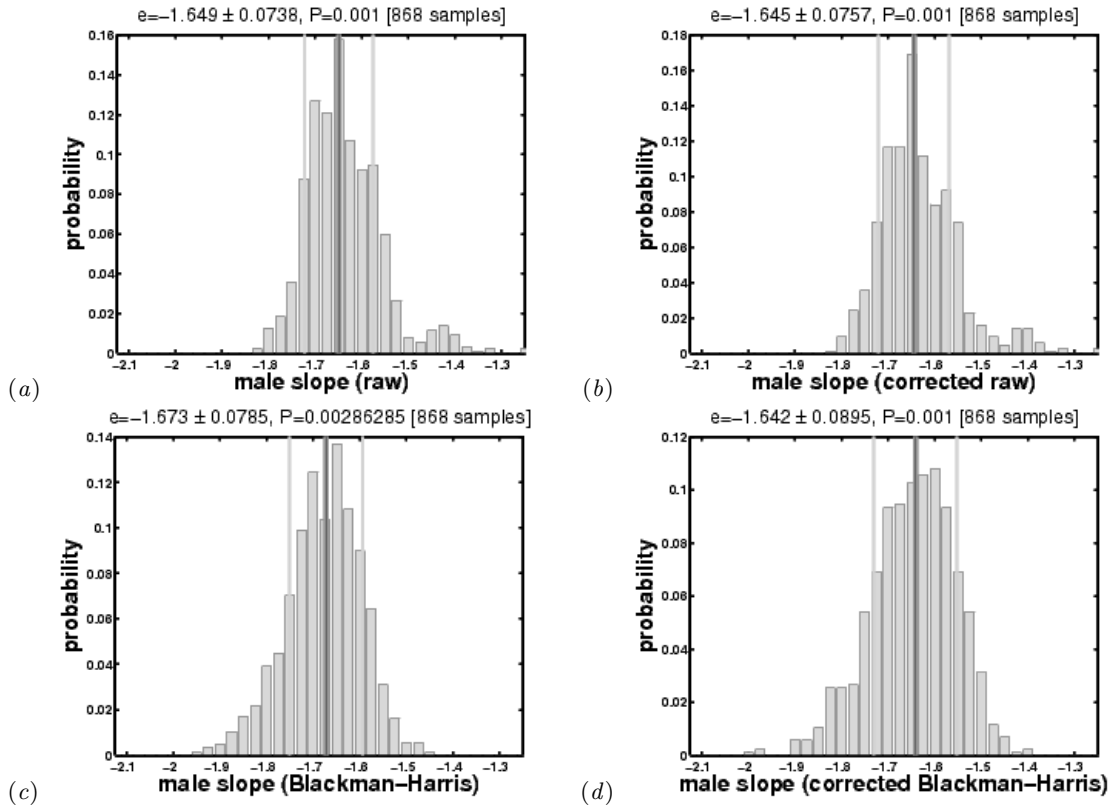


FIG. 9: Slopes for individual images (male faces). The histograms show the probability of occurrence of slope values $e \equiv \alpha$ across all 868 male face images. For each face image, a corresponding slope value was obtained from fitting a line to the double-logarithmic representation of its isotropic 1-D amplitude spectrum (frequency range for fitting from 8 to 100 cycles per image). The centered vertical line in each histogram is the average α , and the flanking lines denote ± 1 s.d., respectively. A Jarque-Bera test was used to test the slope values for normal distribution (this test could be applied because of our large sample size) – corresponding P -values are indicated with each histogram. Corresponding histograms for female images are similar. (a) Raw spectrum: $\alpha = -1.649 \pm 0.0738$, $P < 0.001$. (b) Corrected raw: $\alpha = -1.645 \pm 0.0757$, $P < 0.001$. (c) Blackman-Harris: $\alpha = -1.673 \pm 0.0785$, $P = 0.03$. (d) Corrected Blackman-Harris: $\alpha = -1.642 \pm 0.0895$, $P < 0.001$.

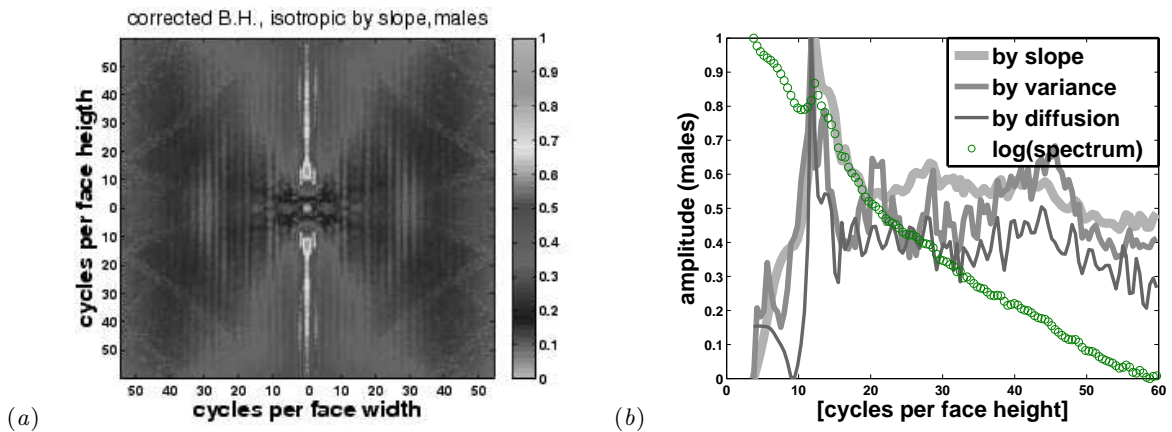


FIG. 10: Whitening by slope. Analogous to figure 4, but for face images of males.

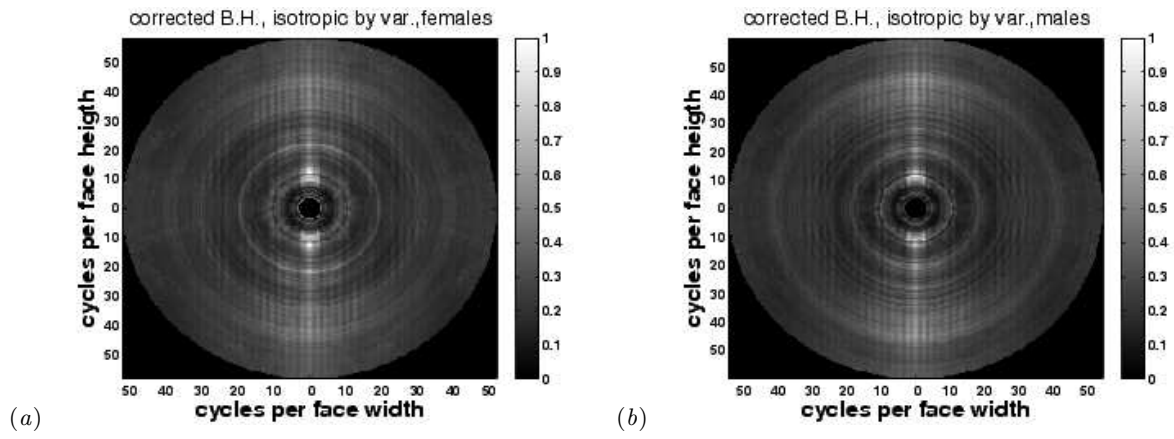


FIG. 11: **Whitening by variance.** Analogous to figure 4(a) (females - left panel) and figure 10(a) (males - right panel) but here for variance-whitening. Again, as with the slope-whitened spectra, maxima are revealed at low spatial frequencies for horizontally oriented features (as indicated by the white regions close the center).